

Neuron, Volume 72

Supplemental Information

Long-Range Neuronal Circuits

Underlying the Interaction

between Sensory and Motor Cortex

Tianyi Mao, Deniz Kusefoglou, Bryan M. Hooks, Daniel Huber, Leopoldo Petreanu, and Karel Svoboda

Inventory of Supplemental Information

1. Figure S1 related to Figure 1
2. Figure S2 related to Figure 1
3. Figure S3 related to Figure 1
4. Figure S4 related to Figure 1, Figure 2 and Figure 3
5. Figure S5 related to Figure 2, Figure 3, and Figure 6
6. Figure S6 related to Figure 4, Figure 5, Figure 6 and Figure 7
7. Figure S7 related to Figure 6
8. Figure S8 related to Figure 6
9. Figure S9 related to Figure 7
10. Table S1 related to Figure 1, Figure 2, Figure 4, Figure 5, Figure 6 and Figure 7
11. Movie S1 related to Figure 1 and Figure S1.
12. Supplemental Discussion
13. Supplemental Experimental Procedures
14. Supplemental References

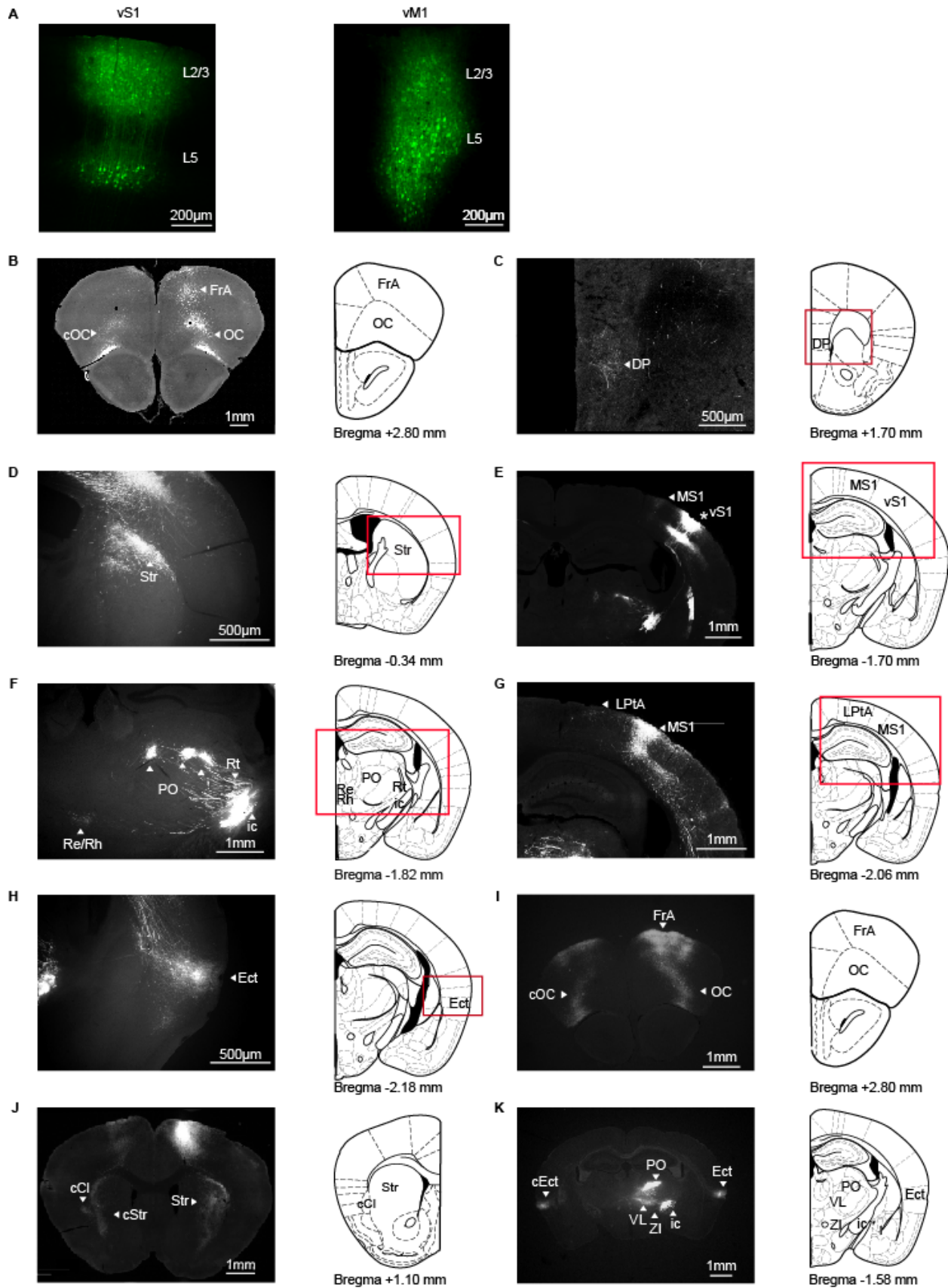


Figure S1. Anterograde tracing with AAV virus.

(A) Example injection sites in vS1 (left) and vM1 (right). In all experiments the injection was in the right hemisphere.

(B) - (H) Fluorescence images of vS1 axons projecting to selected targets and corresponding sections from a standard brain atlas (Paxinos and Franklin, 2004).

(I) - (K) Fluorescence images of vM1 axons projecting to selected targets.

FrA, frontal association cortex; OC, orbital cortex; cOC, contralateral side of orbital cortex; DP, dorsal peduncular cortex; Str, striatum; MS1; medial primary sensory cortex, medial to vS1; vS1, barrel cortex; PO, posterior thalamic nucleus; Rt, reticular thalamic nucleus; ic, internal capsule; Re, reuniens thalamic nucleus and Rh, rhomboid thalamic nucleus; LPtA, lateral parietal association cortex; Ect, ectorhinal/perirhinal cortex; cStr, contralateral side of striatum; cCl, contralateral side of claustrum; ZI, zona inserta; VL, ventral lateral thalamic nucleus.

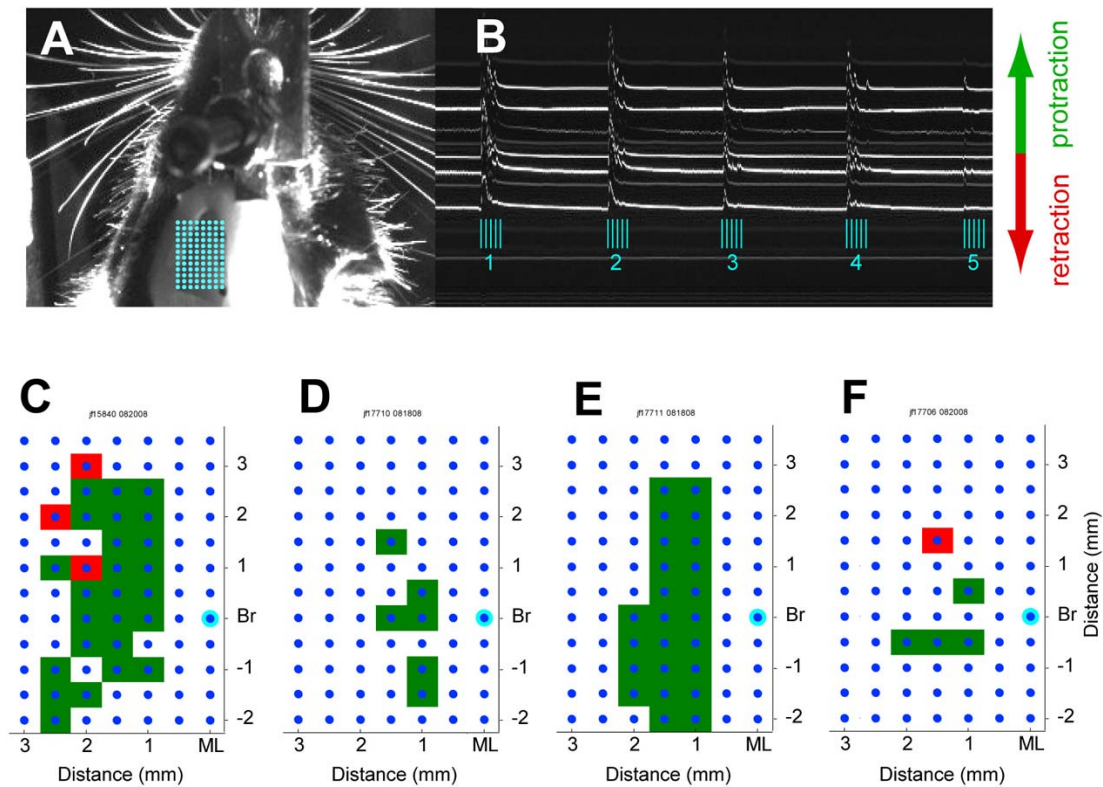
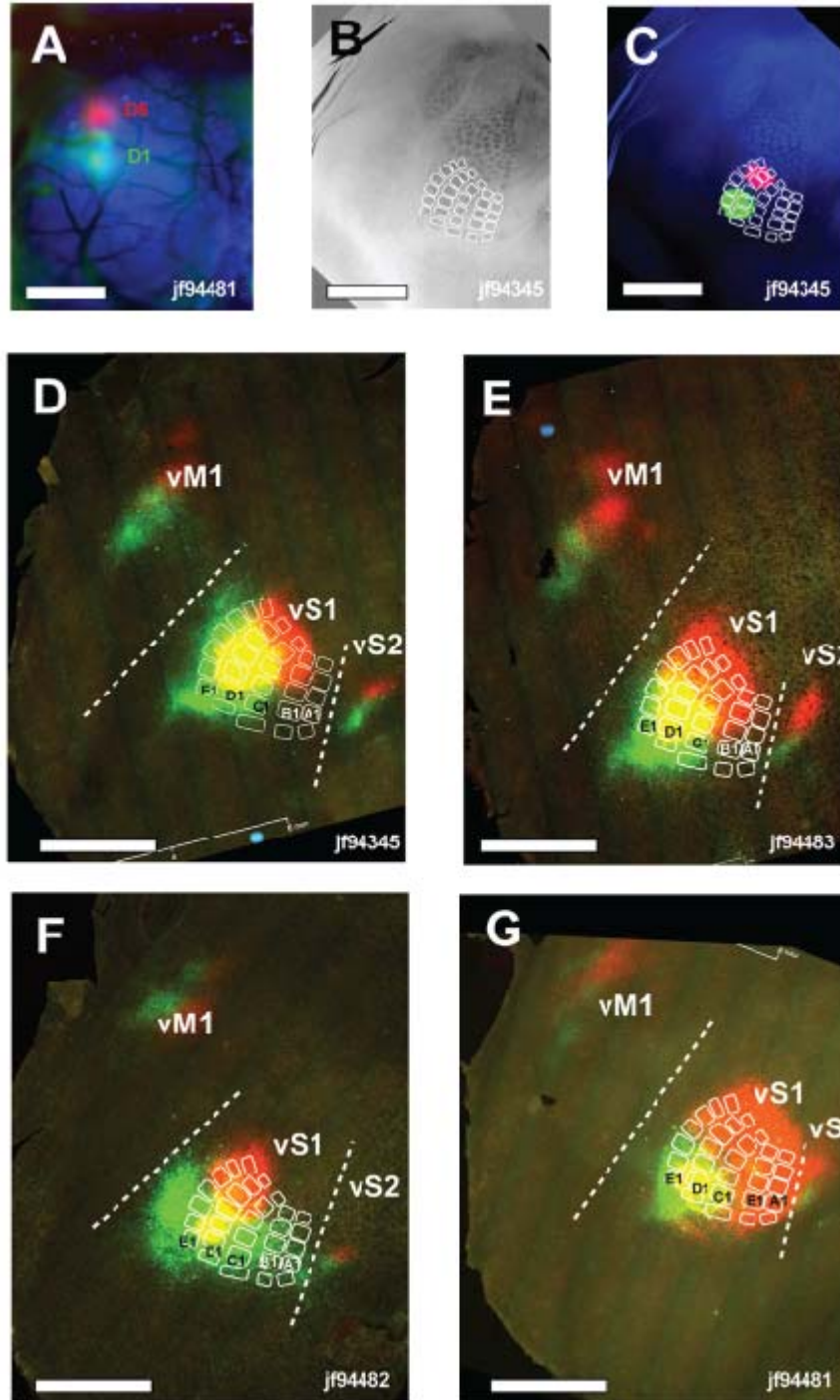


Figure S2. Optical microstimulation in anesthetized mice.

(A) Top view of the mouse head, with the skull exposed over the motor cortex, with the overlaid grid of stimulation locations (blue dots, 8 x 10 grid, 0.5 mm grid spacing).

(B) Whisker movement evoked by optical microstimulation (5 pulses, 5 ms at 20 Hz). Numbers correspond to different points on the stimulus grid. Images of the whiskers were acquired using a high-speed camera (200 Hz).

(C) - (F) Spatial maps of whisker movement in four different mice. Green, protractions. Red, retractions. Br: Bregma, ML: Midline. Photostimulation is less effective close to the midline because of the curving brain geometry and the overlying vasculature.



H

	Animal #1	Animal #2	Animal #3	Animal #4	Mean ± SEM
Distance between injection sites (µm)	872.8	433.6	757.6	1135.4	799.8 ± 145.4
Distance between projection sites (µm)	658.0	231.4	600.7	740.0	557.4 ± 112.3
Ratio	1.33	1.87	1.26	1.54	1.490 ± 0.14

Figure S3. Topography of vS1 → vM1 projections in flat mounts.

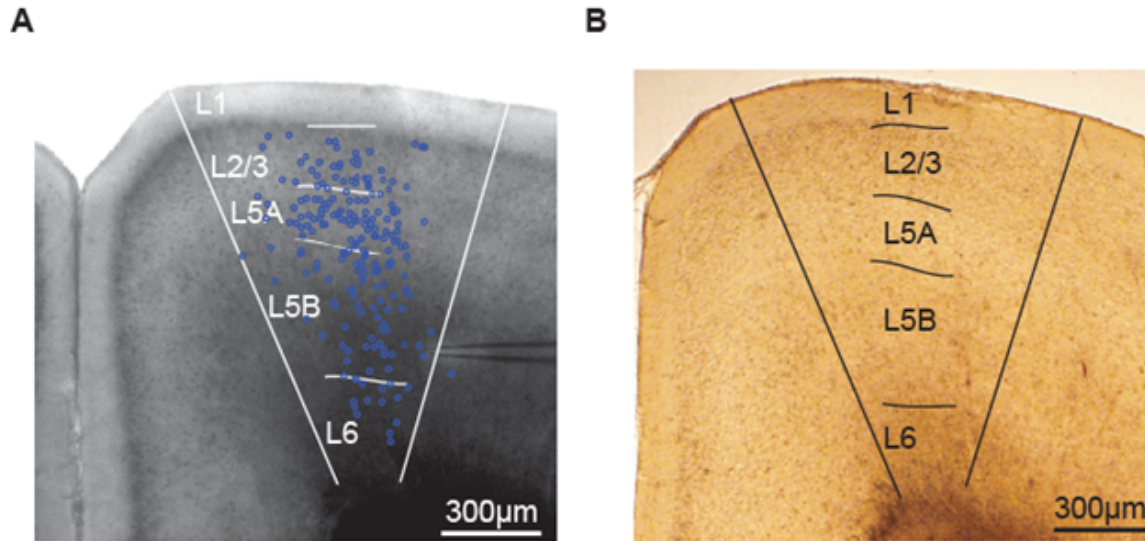
(A) Intrinsic optical signals produced by deflection of D1 (green) or D5 (red) whiskers were imaged through the skull. These images guided subsequent viral injections.

(B) Barrel field in a flatmount. Scale bar, 1mm.

(C) Overlay of the barrel field and two injection sites (AAV viruses expressing GFP and tdTomato respectively). Scale bar, 1mm.

(D) - (G) Images of cortical flat mounts. Viral infection was in the D1 (green, GFP) and D5 (red, tdTomato) barrels of vS1. The barrel field is outlined in white. The major terminal fields in secondary somatosensory cortex (S2) and motor cortex (vM1) are separated with dashed white lines. Scale bars, 1mm.

(H) Quantification of the distances between injection sites, projections sites, and the ratios of the two distances (distance in vS1 divided by distance in vM1; also see Supplemental Experimental Procedures).



C

	Relative depth	Absolute depth (μm)
L1	0.11 ± 0.01	160 ± 17
L2/3	0.26 ± 0.04	380 ± 53
L5A	0.40 ± 0.02	600 ± 42
L5B	0.78 ± 0.04	1145 ± 65
L6	NA	1448 ± 30
	N=17	N=17

Figure S4. Cortical layers and recording locations in vM1.

(A) Bright field image of a vM1 brain slice. The vertical lines demarcate the recording locations. Horizontal lines indicate layers. Blue dots represent the relative locations of all cells recorded for this study ($n = 210$).

(B) A fixed vM1 brain slice after 3,3-diaminobenzidine (DAB) treatment.

(C) The depths of the bottom boundaries of cortical layers (for criteria see the main text) measured across $N=17$ brain slices. Relative depth is normalized to pia (0) and white matter (1). Note that upper layers are relatively more contracted closer to the midline (Hooks et al., 2011).

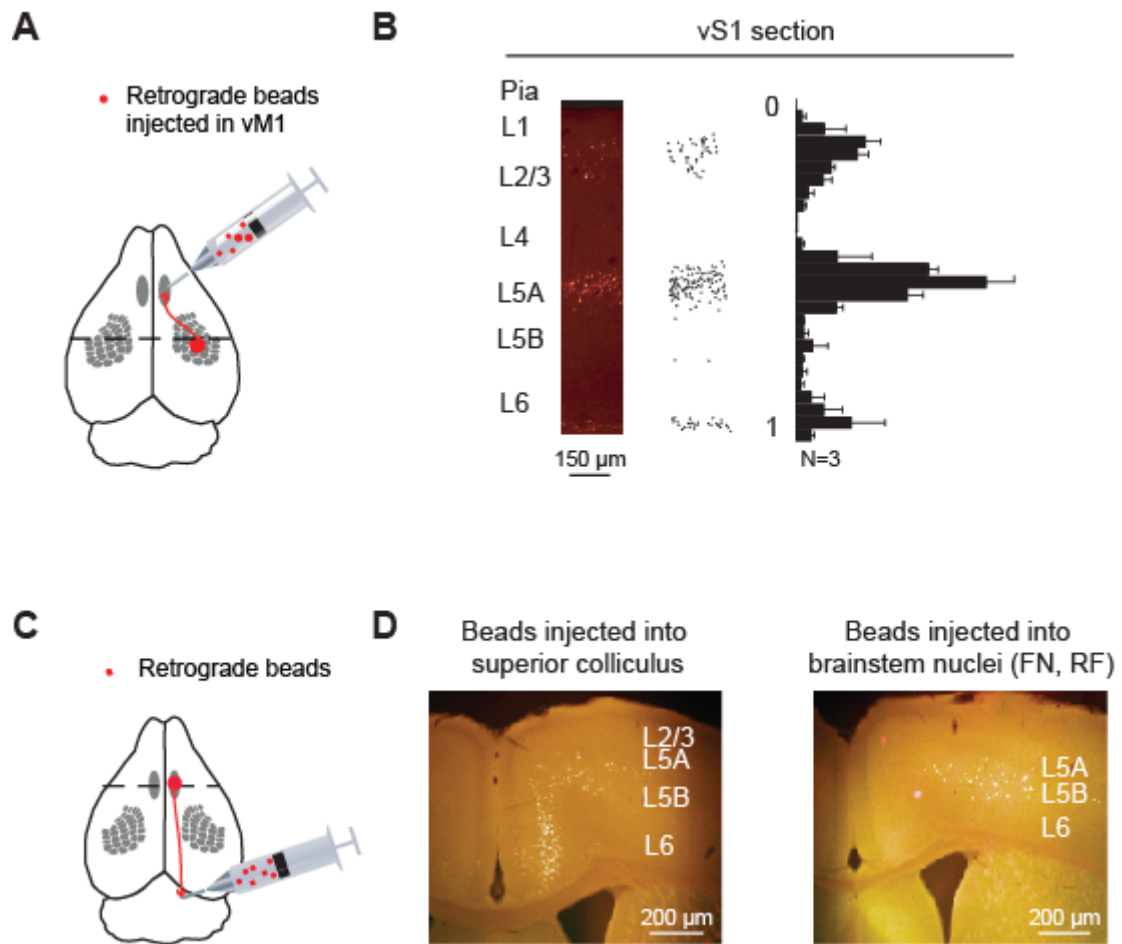


Figure S5. Retrograde labeling experiments.

(A) - (B) Microbeads injected in vM1 (A), bead counting in vS1 (B) (section corresponding to dashed line in A).

(C) - (D) Microbeads injected in superior colliculus or brainstem (C), images in vM1 (D) (section corresponding to dashed line in C). FN, facial nucleus; RF, reticular formation.

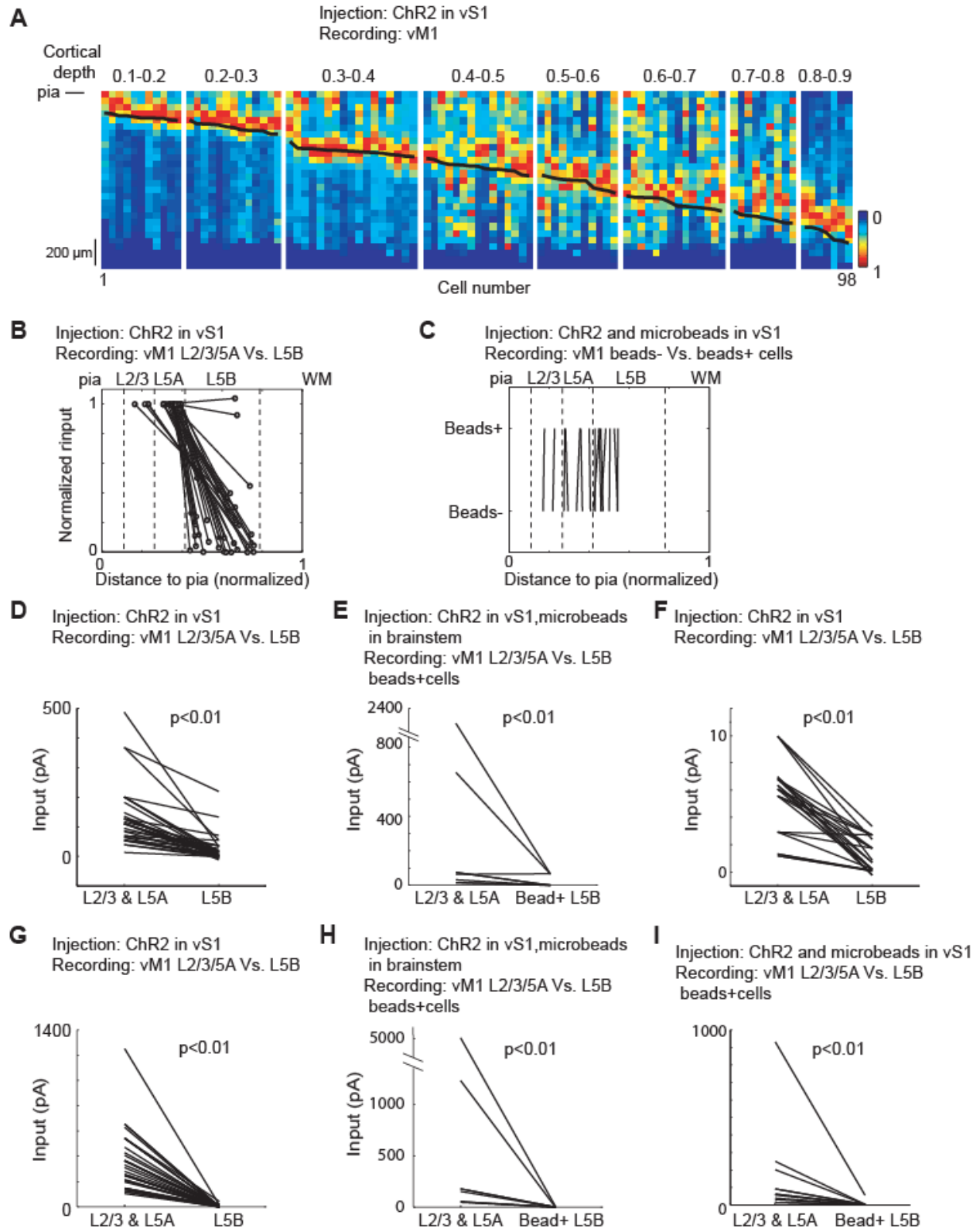


Figure S6. vS1 input to vM1 cells.

(A) Vertical profiles of sCRACM maps for individual cells recorded in vM1. Each column corresponds to a cell's input map, averaged along the horizontal dimension. Black line indicates the soma position.

(B) Normalized input for pairs of cells recorded at different cortical depths. L5B cells in vM1 received low input from vS1 compared to upper layer cells (same data as in Figure 6A, C). WM, white matter.

(C) Cortical depth of pairs of bead+ and neighboring bead- cells (same cells as in Figure 7E).

(D) - (F) Same data as in Figure 6, but input was calculated as the sum of the 3 x 3 pixels nearest to the soma. (D) Injection in vS1; recording in vM1. Input to upper layer neurons (L5A and L2/3) compared to L5B. (E) Injection in vM1 (ChR2) and brainstem (microbeads); recording in vM1. (F) CRACM input: same experiments as (A), except with NMDA-Rs, Na channels, and K channels intact (CPP, TTX, and 4-AP omitted from the bath).

(G) - (I) Input was calculated using a mask defined by a map averaged across the cells within a group. For individual cells, input was then calculated by summing pixels across the mask (see Experimental Procedures). (G) Same data as in (D). (H) Same data as in (E). (I) Injection: ChR2 and microbeads in vS1; recording: vM1. vS1-projecting L5B cells in vM1 (bead+) and upper layer cells (L2/3 & L5A) receiving input from vS1 were compared.

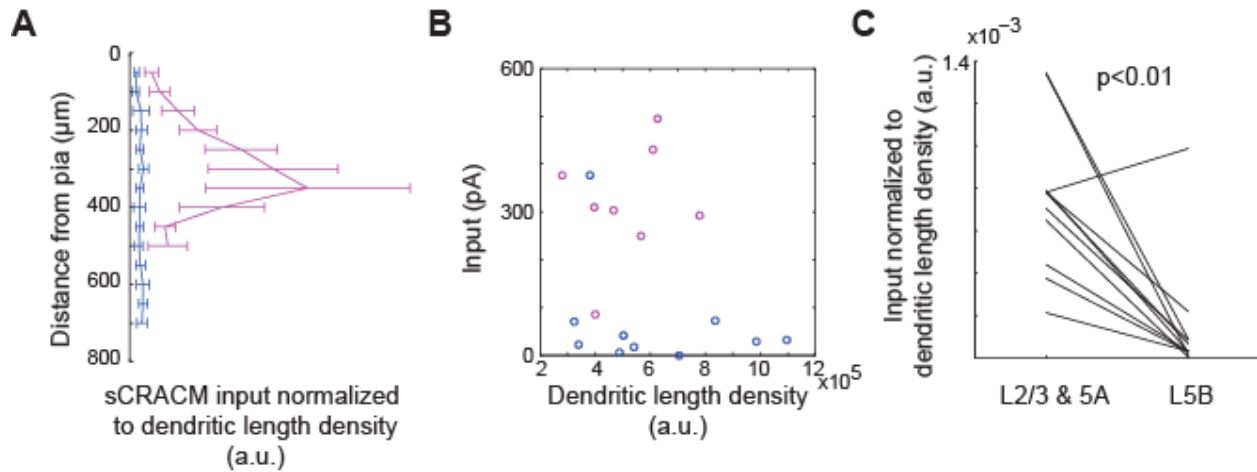


Figure S7. Specificity of vS1 input.

(A) L5A cells receive more vS1 input for the same unit of dendritic length. Responses of L5A cells (magenta, $n=19$ cells, 13 animals) and L5B cells (blue, $n=15$ cells, 11 animals) divided by dendritic length density, averaged across the cells within the group, and plotted against depth in the brain slice. Error bars, SEM.

(B) Input from vS1 to upper layer cells in vM1 (L5A and L2/3, magenta circles, $n=8$ cells, 7 animals) and paired L5B cells (blue circles, $n=10$ cells, 7 animals) in vM1, plotted against dendritic length density.

(C) Input from vS1 to upper layer cells normalized to dendritic length density and compared with paired L5B cells ($n=11$ pairs of cell, 7 animals; $p < 0.01$, non-parametric signed-rank test).

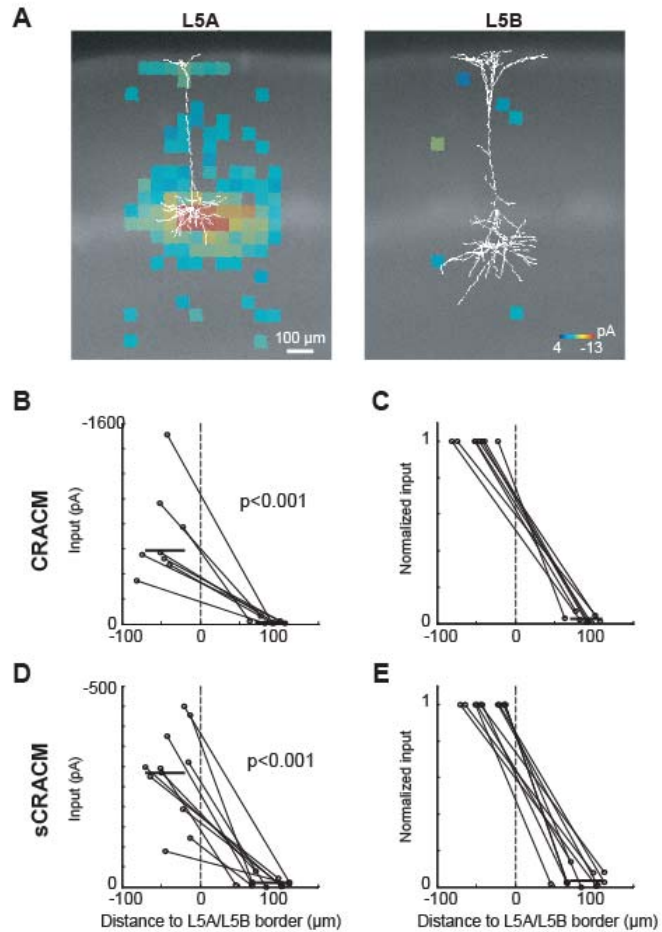


Figure S8. Comparison of input from PO to L5A and L5B in vS1.

(A) Neurons in PO were labeled with Chr2-GFP. The axons terminate in L5A and L1 in vS1. Overlaid on the reconstructions of dendritic arbors from individual neurons are CRACM input maps to a L5A (left) and a neighboring L5B (right) pyramidal neuron. Blockers of NMDA-Rs, Na channels, and K channels were omitted in this experiment

(B) Total input (sum of all pixels in the CRACM map) from PO for pairs of neighboring L5A and L5B neurons recorded under identical stimulation conditions. Horizontal line indicates mean values. CRACM input, mean, range: L5A, -713 pA, -1509- to -346 pA; L5B, -19, -65 to -4 pA.

(C) Same data as in (B), normalized to the total pixel value of CRACM input to L5A neurons. Ratio of CRACM input (L5B/L5A), mean, range: 0.026, 0.068-0.008.

(D) Analysis same as (B) but for sCRACM maps (Blockers of NMDA-Rs, Na channels, and K channels were included in this experiment). sCRACM input, mean, range: L5A, -283 pA, -449 to -88 pA; L5B, -10 pA, -39 to 0 pA. See also Petreanu et al. 2009.

(E) Analysis as in (C), data as in (D). Ratio of sCRACM input (L5B/L5A), mean, range: 0.038, 0.14-0.

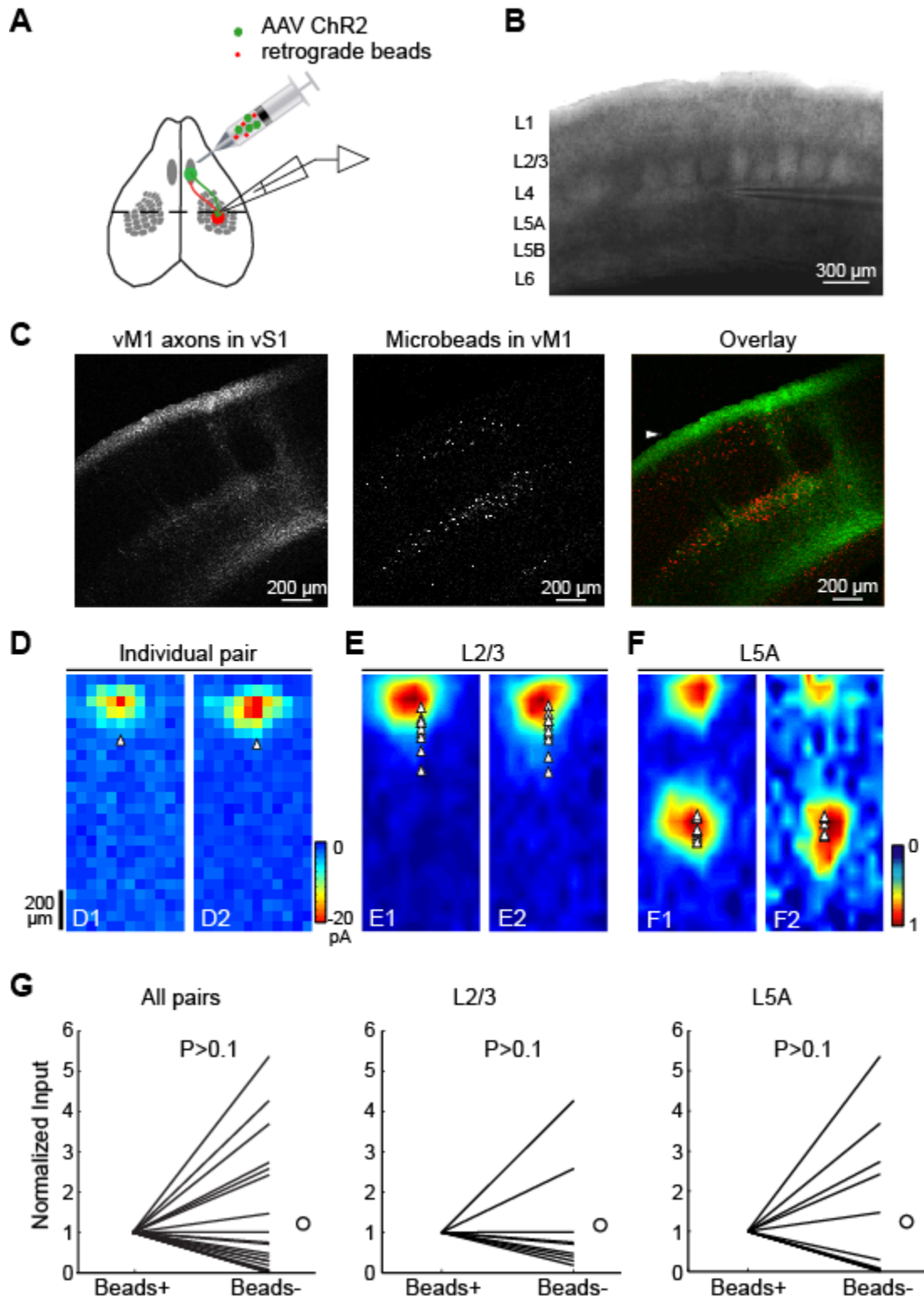


Figure S9. vM1-projecting neurons in vS1 receive input from vM1.

(A) Schematic of the experiment. AAV-ChR2 (green) and fluorescent microbeads (red) were co-injected into vM1. Recordings were made in vS1 (dashed line).

(B) Bright field image of a vS1 brain slice.

(C) Representative images of vM1 axons (left), bead-labeled cells (vM1-projecting cells; middle), and the overlay (right) in vS1.

(D) A pair of sCRACM input maps recorded from a bead-positive cell (vM1-projecting, D1) and a neighboring bead-negative cell (soma distance less than 50 μ m, D2) (triangle, soma location).

(E) Average sCRACM maps for bead-positive L2/3 neurons in vS1 (E1) and their neighboring bead-negative neurons (E2), aligned by pia.

(F) Average sCRACM maps for bead-positive L5A neurons in vS1 (F1) and their paired bead-negative neurons (F2), aligned by pia.

(G) Comparison of vM1 input to bead-positive and nearby (distance < 50 μ m) bead-negative cells for all cortical layers (left, n=22 pairs of cells, 14 animals), for L2/3 cells only (middle, n=9 pairs of cells, 7 animals) and for L5A cells only (right, n=13 pairs of cells, 9 animals) in vS1. Bead-negative cells' input is normalized to the paired bead-positive cells. Large circles indicate the mean of normalized input values of each cell group.

Supplemental Table

Table S1: Summary of total animal numbers and cell numbers used in the quantifications.

Figure	# of animals	# of cells	# pairs	Comments
1B1-1B3	N=10	NA	NA	
1C	N=3	NA	NA	
1E	N=4			
1G1-1G3	N=10			
1H	N=2	NA	NA	
2C	N=15	NA	NA	N=3 for each group
4C	N=11	N=34	N=19	
4D	N=15	N=52	N=31	
4E	N=8	N=24	N=21	
4F	N=24	N=97	N=72	
5A	N=35	N=77	NA	
5B (map)	N=35	N=77	NA	Same data as 5A
5B (reconstruction)	N=19	N=46	NA	
6A	N=17	N=59	N=36	
6B	N=4	N=19	N=23	
6D	N=5	N=13	N=8	
7E	N=12	N=30	N=15	

Supplemental Experimental Procedures:

Stereotactic injections

For sCRACM experiments, we injected ChR2-expressing virus into one site in vS1 and two nearby sites in vM1. At each site, 20 – 40 nl of virus was injected at two depths, 350 - 400 μm and 600 - 750 μm . Co-injections of virus and microbeads were performed in two different ways: simultaneous co-injection of a mixture of virus and beads (2 x 40-80 nl), or injection of virus as above, followed 10 days later by microbeads (2x 20-40 nl) at the same site. For anterograde tracing, 6 week old animals were injected with AAV expressing CAG-tdTomato or CAG-eGFP into vS1 or vM1. Injection volumes were 10 nl each at two depths (Figure 1). For dual color viral injections (Figures 1D-1E), 10-15 nl virus was injected at depths of 300 and 800 μm in specific regions of vS1, guided by intrinsic optical signal imaging (O'Connor et al., 2010).

Slice preparation

Brain slices were prepared 14 to 24 days after viral infection (postnatal day 27-39). Mice were deeply anesthetized with ketamine (6.25 mg/ml) and xylazine (1 mg/ml) and perfused transcardially with cold artificial cerebrospinal fluid (ACSF) (in mM: 127 NaCl, 25 NaHCO₃, 25 D-Glucose, 2.5 KCl, 2 CaCl₂, 1 MgCl₂, 1.25 NaH₂PO₄). The brain was rapidly removed from the skull and placed in chilled cutting solution containing (in mM): freshly added 110 choline chloride, 3.1 sodium pyruvate, 11.6 sodium ascorbate and stock solution of 25 NaHCO₃, 25 D-glucose, 7 MgCl₂, 2.5 KCl, 1.25 NaH₂PO₄, 0.5 CaCl₂). Slices (300 μm) were incubated for 30 to 45 minutes at 37 °C in oxygenated ACSF and maintained in a holding chamber at room temperature (22 °C to 24°C).

Reconstructions of dendritic arbors

Slices with biocytin-filled neurons were fixed in 4% paraformaldehyde. After labeling (ABC kit, Vector Lab), slices were stained with 3,3-diaminobenzidine (DAB) and coverslipped in AquaPolymount (Polysciences) or Fluoromount (Sigma). Dendrites were reconstructed using NeuroLucida (MicroBrightField) using a 40x objective and analyzed using custom software

written in Matlab. NeuroLucida tracings were corrected for shrinkage due to fixation. The correction factor for each cell was calculated by comparing the distance of the soma to the pia before and after the fixation. Dendritic length density was calculated from the reconstructed dendrites. For the group averages of dendritic length density (Figure 5B), peak normalized length-density maps were aligned on the soma. The bin size was 50 μm to match the sCRACM mapping resolution.

Counting fluorescent microbeads

To estimate cellular distributions in retrograde labeling experiments, we acquired fluorescence images and counted bead-positive somata with NeuroLucida. Labeled cells were not uniformly filled with microbeads, and the correspondence between bead clusters and individual neurons was therefore sometimes ambiguous. However, estimates of densities of labeled neurons were consistent across different human analyzers (data not shown). Comparisons of densities of labeled neurons across locations are likely robust (Figure 2B).

Histology and fluorescence imaging

Two weeks after viral infection, mice were perfused transcardially with 4% paraformaldehyde (PFA) followed by further PFA fixation for 24 hours. Brains were embedded in 5% agarose and sectioned with the vibratome (Leica 1000) or embedded in Optimal Cutting Temperature (OCT) medium (TISSUE-TEK) sectioned on the cryostat (50 μm thick sections). Sections were imaged with a slide scanner (Nanozommer, Hamamatsu) (Figures 1E, S1, S4 and Table S2), a MVX microscope (Olympus) (Figures 1B1-B3 and D1-D3, 7B and S1), a confocal laser scanning microscope (Zeiss 510) (Figures 1B4, D4, S1A, and S10C) and Zeiss Axioimager Z1 (Figure 1C).

For cortical flat-mounts (Figure 1E and Figure S3) mice were perfused with 1% PFA. The entire cortex of the injected hemisphere was extracted, unfolded and gently compressed between two glass slides (Sincich et al., 2003). After post-fixation with 4% PFA, the tissue was cryo-protected with 30% sucrose and cut on a cryostat (section thickness, 40 μm). For some experiments (Figures 1B, 4, 5, 6, 7, and S1B-H) the injection sites were referenced to the barrel field with cytochrome oxydase staining (Feldbauer et al., 2009). For quantification of the distance between

the injection sites in vS1 and their corresponding vM1 projection sites in each animal, we calculated the center of the fluorescence intensity in green and red channels and their distances (Figure S3H).

For quantification of projection strength (Figure 1E and Table S2), the entire brain was sectioned coronally (50 μ m). Sections were mounted on microscope slides and native fluorescence was imaged using a slide scanner (Nanozoomer, Hamamatsu). The illumination was adjusted so that the brightest regions across the brain did not saturate the CCD camera. Images were quantified using Matlab scripts. Regions of interest (ROIs) were selected to surround distinct axonal projection zones. Background was calculated by averaging intensity values in corresponding areas in the contralateral hemisphere, or, for bilateral projections, over regions immediately adjacent to the ROI. After background subtraction, the fluorescence intensity was summed over each ROI and across sections to produce an estimate of projection strength. Each projection zone was assigned to a brain area according to a standard mouse brain atlas (Paxinos and Franklin, 2004). The quantification of projection strength assumes that the fluorescent proteins label neurons homogeneously and that axonal boutons are homogeneously distributed along the axon (Anderson et al., 2002).

Some notes regarding definitions of the ROIs for quantifications of vS1 outputs. Projections to S2 appeared as a distinct band of fluorescence, separate from the vS1 injection site and projections within vS1. Projections to vM1 were continuous with weaker projections to prefrontal areas (FrA). Because we did not see a clear demarcation point these projections were grouped. For projections to the striatum, we tried to exclude strongly fasciculated axons, likely axons of passage. However, in a few instances fasciculated axons were intermingled with axonal termination zones with clear boutons and were thus included. As a consequence, projections to the striatum tend to be overestimated. For projections to contralateral S1, we measured all of the fluorescence in S1. For projections to ectorhinal/perirhinal cortical areas, a band of fluorescence was parallel to the horizontal axis, including the rhinal fissure. For projections to thalamus we did not distinguish between different nuclei except Rh/Re and ZI, because these locations were clearly separated from the rest of thalamus. For ZI, we excluded the axons of passage in the cerebral peduncle.

Some notes for vM1 outputs. Since the boundary between vM1 and FrA was indistinct, projections to FrA might include projections within vM1. Contralateral side of claustrum (cCl) contained a distinct projection zone along the outside rim of the external capsule. For projections to vS1, we calculated all the fluorescence in sensory cortex, including S2.

Supplemental References:

Anderson, J.C., Binzegger, T., Douglas, R.J., and Martin, K.A. (2002). Chance or design? Some specific considerations concerning synaptic boutons in cat visual cortex. *J Neurocytol* 31, 211-229.

da Costa, N.M., and Martin, K.A. (2009). The proportion of synapses formed by the axons of the lateral geniculate nucleus in layer 4 of area 17 of the cat. *J Comp Neurol* 516, 264-276.

Feinberg, E.H., Vanhoven, M.K., Bendesky, A., Wang, G., Fetter, R.D., Shen, K., and Bargmann, C.I. (2008). GFP Reconstitution Across Synaptic Partners (GRASP) defines cell contacts and synapses in living nervous systems. *Neuron* 57, 353-363.

Feldbauer, K., Zimmermann, D., Pintschovius, V., Spitz, J., Bamann, C., and Bamberg, E. (2009). Channelrhodopsin-2 is a leaky proton pump. *Proc Natl Acad Sci U S A* 106, 12317-12322.

Hamos, J.E., Van Horn, S.C., Raczkowski, D., and Sherman, S.M. (1987). Synaptic circuits involving an individual retinogeniculate axon in the cat. *J Comp Neurol* 259, 165-192.

Hooks, B.M., Hires, S.A., Zhang, Y.X., Huber, D., Petreanu, L., Svoboda, K., and Shepherd, G.M. (2011). Laminar analysis of excitatory local circuits in vibrissal motor and sensory cortical areas. *PLoS Biol* 9, e1000572.

Micheva, K.D., Busse, B., Weiler, N.C., O'Rourke, N., and Smith, S.J. (2010). Single-synapse analysis of a diverse synapse population: proteomic imaging methods and markers. *Neuron* 68, 639-653.

Micheva, K.D., and Smith, S.J. (2007). Array tomography: a new tool for imaging the molecular architecture and ultrastructure of neural circuits. *Neuron* 55, 25-36.

O'Connor, D.H., Peron, S.P., Huber, D., and Svoboda, K. (2010). Neural activity in barrel cortex underlying vibrissa-based object localization in mice. *Neuron* 67, 1048-1061.

Paxinos, G., and Franklin, H.B.J. (2004). *The Mouse Brain in Stereotaxic Coordinates: Compact Second Edition* (Amsterdam, Elsevier).

Petreanu, L., Huber, D., Sobczyk, A., and Svoboda, K. (2007). Channelrhodopsin-2-assisted circuit mapping of long-range callosal projections. *Nat Neurosci* 10, 663-668.

Petreanu, L., Mao, T., Sternson, S.M., and Svoboda, K. (2009). The subcellular organization of neocortical excitatory connections. *Nature* 457, 1142-1145.

Sincich, L.C., Adams, D.L., and Horton, J.C. (2003). Complete flatmounting of the macaque cerebral cortex. *Vis Neurosci* 20, 663-686.

Spruston, N., Jaffe, D.B., Williams, S.H., and Johnston, D. (1993). Voltage- and space-clamp errors associated with the measurement of electrotonically remote synaptic events. *J Neurophysiol* *70*, 781-802.

White, E.L., and DeAmicis, R.A. (1977). Afferent and efferent projections of the region in mouse SmL cortex which contains the posteromedial barrel subfield. *J Comp Neurol* *175*, 455-482.

Williams, S.R., and Mitchell, S.J. (2008). Direct measurement of somatic voltage clamp errors in central neurons. *Nat Neurosci* *11*, 790-798.